

LASER EXPERIMENT TO STUDY RADIATIVE SHOCKS RELEVANT TO ASTROPHYSICS.

U. Chaulagain¹, C. Stehl e¹, J. Larour², M. Kozlova³, P. Barroso⁴, L. de Sa^{1,5}, F. Suzuki-Vidal⁶, O. Acef⁷, P. Auvray², M. Krus^{3,8}, J. Dostal³, J. Prokupek^{3,8}, F. Reix⁴ and A. Ciardi¹

Abstract. We present results of recent laboratory experiments on radiative shocks in xenon at low pressure. The shocks are generated with the high energy, sub-nanosecond laser at PALS, European facility. The main diagnostic consists of instantaneous imaging of the whole shock structure using an X-ray laser at 21.2 nm. The shock timing is also analyzed with time-and-space resolved plasma self-emission using high speed diodes. The achieved shock velocities near 50 kms⁻¹ are sufficient to generate a radiative shock characterized by the development of a radiative precursor.

Keywords: Radiative shocks, plasma physics, XUV laser, stellar formation, accretion processes.

1 Introduction

Radiative accretion shocks occur in different stages of stellar evolution, for instance, during stellar infancy where the stellar core accretes matter from its surroundings (Commerçon et al. 2011) or in already formed young stars (Bouvier et al. 2007). In the case of accretion shocks in young classical T Tauri stars, the gas is funneled from the circumstellar disk onto the photosphere along the magnetic field lines falling onto the star at the free fall velocity, i.e. at about 400 kms⁻¹. This generates a strong shock which has specific spectral signatures, for instance, emission in the X-ray region (Argiroffi et al. 2007).

These hypersonic accretion shocks are strongly structured by radiation. However, the regime for radiation transport depends on the location of the shock in the stellar atmosphere and may vary between optically thin and optically thick regimes. The first case occurs if the shock is formed in the low density upper chromosphere, and it is characterized by strong post shock radiative cooling. The second case occurs when the shock is formed in the deeper and denser layers of the atmosphere. In this case, the intense radiation emerging from the shock front, which is heated to very high temperature, ionizes and heats the cold upstream gas and will form an ionization wave called ‘radiative precursor’ (Zeldovich & Zel’dovich 2002). The complicated coupling between hydrodynamics and radiation makes these shocks precious test bench for radiative-hydrodynamic codes (Gonzalez et al. 2009) and strongly motivates their experimental study.

Radiative shock experiments can be performed at high energy laser facilities (Bouquet et al. 2004; Reighard et al. 2006; Stehl e et al. 2010). A typical laser irradiance of 10¹⁴ Wcm⁻² or more allows in few ns to launch radiative shocks in gas cells (Doss et al. 2009; Stehl e et al. 2010) with xenon. Optimal pressure for this purpose is a fraction of 1 bar. Hence, the achieved temperature of the shock is higher for heavier gases at a given shock

¹ LERMA, Observatoire de Paris - Universit e Pierre et Marie Curie - ENS - Universit e de Cergy Pontoise - CNRS, 5 Place J. Janssen, 92195 Meudon, FR

² LPP, Ecole polytechnique, UPMC, CNRS, Palaiseau, FR

³ Institute of Physics, Prague, Czech Republic, CZ

⁴ GEPI, Observatoire de Paris, University Paris Diderot, CNRS, Paris, FR

⁵ Laboratoire AIM, CEA/DSM/IRFU/SAP - CNRS - Universit e Paris Diderot, Orme des Merisiers, 91191 Gif-sur-Yvette, FR

⁶ Imperial College, London, UK

⁷ SYRTE, Observatoire de Paris, UPMC, CNRS, LNE, Paris, FR

⁸ Czech Technical University in Prague, FNSPE, Czech Republic, CZ

velocity determined by the laser intensity. Nevertheless, many aspects of these experiments are still not fully understood, and thus, there is a need for new diagnostics to measure and constrain some physical parameters of these shocks. Here the results of two complementary diagnostics are presented, namely, instantaneous imaging at a wavelength of 21.2 nm (hereafter called ‘XUV’ imaging) of the whole shock structure and a measurement of the shock velocity using fast diodes. The present results confirm and strongly improve the quality of the results obtained from the previous proof of principle experimental campaigns (Stehlé et al. (2012a,b)).

2 Experimental Setup and Diagnostics

The experiments were performed at the Prague Asterix Laser System (PALS). This facility can deliver up to 1 kJ of energy at a wavelength of 1.315 μm , a pulse duration of 0.35 ns and a repetition rate of 2 shots/hr (Jungwirth et al. 2001). The PALS laser beam was split into two beams during the experiments: AUX & MAIN.

The AUX beam (with an energy of 60 J and pulse duration of 0.35 ns) was used to drive a shock by focusing the beam to a diameter of 300 μm on a piston attached to a miniaturized shock ‘tube’, positioned inside a vacuum chamber. The AUX beam achieved nominal irradiance of $2 \times 10^{14} \text{ Wcm}^{-2}$ on the target. The MAIN beam (energy of 500 J and pulse duration of 0.35 ns) was focused on a zinc planar target located in a separate vacuum chamber. An X-ray laser (XRL, 3 mJ, 0.2 ns) with a wavelength of 21.2 nm is created by the sequence of strong MAIN and weak pre-pulse beams, typical energy ratio between them is 10^3 (Rus et al. 2002). This X-ray laser was used as an instantaneous side-on back-lighter of the shock wave with a fixed delay of 20 ns respect to the AUX beam. A schematic diagram of the experimental setup showing these three lasers is presented on the left in Fig. (1).

The targets consisted of squared channel with typical length of 6 mm and cross-section of $(0.4 \times 0.4 \text{ mm}^2)$. The targets were filled *in situ* with xenon at a pressure of 0.3 bar corresponding to a density of $1.5 \times 10^{-3} \text{ gcm}^{-3}$ at room temperature. The tube is closed on the one end by the piston, a double layer consisting of a polystyrene foil (10 μm thick) with a gold (0.5 μm) coating. The ablation of the polystyrene layer by the AUX laser generates a shock in the gas by rocket effect. The gold layer aims at blocking the X-rays generated by the interaction between the driving laser and the polystyrene. The shock tube is closed laterally by two membranes made of silicon nitride (Si_3N_4) each having a thickness of 100 nm and placed inside a silicon frame. These membranes have a transmission of 13 % at 21.2 nm, i.e. sufficient to allow probing with the XRL beam (Henke et al. 1993).

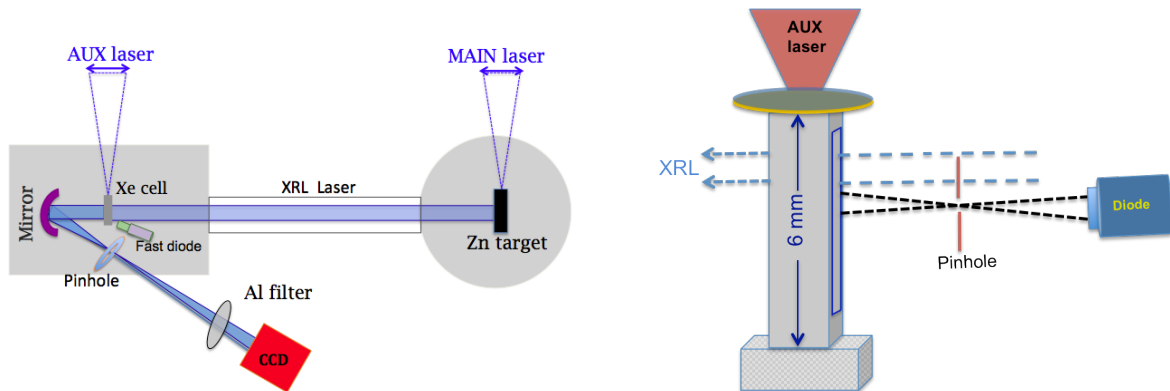


Fig. 1: Schematic experimental setup with three lasers and XRL imaging (*left*), and side view of high-speed diode diagnostics (*right*). The diode provides 1 mm^2 Silicon detector. The distance between pinhole to Si_3N_4 window of shock tube is 7.7 mm and pinhole to detector is 6.8 mm. The axis between diode diagnostics is in plane perpendicular to the axis of the target and makes an angle of 30 degrees with XRL beam. The diode looks through the small section of the window, located at about 1.8 mm from the piston.

The XRL beam passes through the shock tube reaching afterwards a spherical XUV mirror (focal length of 300 mm and diameter of 25.4 mm) which focuses the beam into an iron pinhole (diameter = 500 μm). This pinhole blocks the plasma self-emission by reducing the numerical aperture of the imaging system. This also

efficiently reduces the aberrations of the spherical mirror with non-normal incidence. Finally, the XRL beam reaches the cooled CCD filtered with a 10 μm thick aluminium foil which blocks the parasitic visible light (see Fig. 1 on the left). The target is projected with a magnification of 4.8 (Stehlé et al. 2012c; Chaulagain et al. 2012). Since the wavelength of the XRL beam is small compared to the aperture of the optics and the object, any diffraction effects due to the illumination of the object by the XRL beam have a negligible impact on spatial resolution.

The size and alignment of laser focal spot which drives the shock is an important parameter, as it can directly affect the dynamics and symmetry of the shock inside the tube during the experiments. In order to characterise the position and size of the laser spot, the AUX laser, attenuated by 10% gray filter, was also shot onto solid aluminium targets mimicking the experimental targets. The X-ray radiation emitted from the interaction was monitored by a keV pinhole camera. The crater size generated from the laser-target interaction insured a good level of alignment on target (Chaulagain et al. 2012). From these measurements, the laser spot size during the experiments is expected to be about 300 μm .

Silicon diodes were used to record the time-dependent self-emission from the plasma at a fixed position along the shock tube, and thus, estimate the shock velocity (see on the right in Fig. 1). The diodes were located side-on from the shock tube and tilted at an angle of 30 degrees, in order to not block the line of sight of the XRL beam. The diodes had a detection area of 1 mm^2 and a response time of 1 ns, and were positioned at about 14.5 mm from the axis of the shock channel. A tungsten pinhole with a diameter of 200 μm provided spatial resolution and was located at a distance of 6.8 mm from the shock channel. Lastly the diode had an integrated aluminium filter coating in order to record the self emission from the shock in XUV region.

3 Results

3.1 XUV imaging of the shock with XRL laser

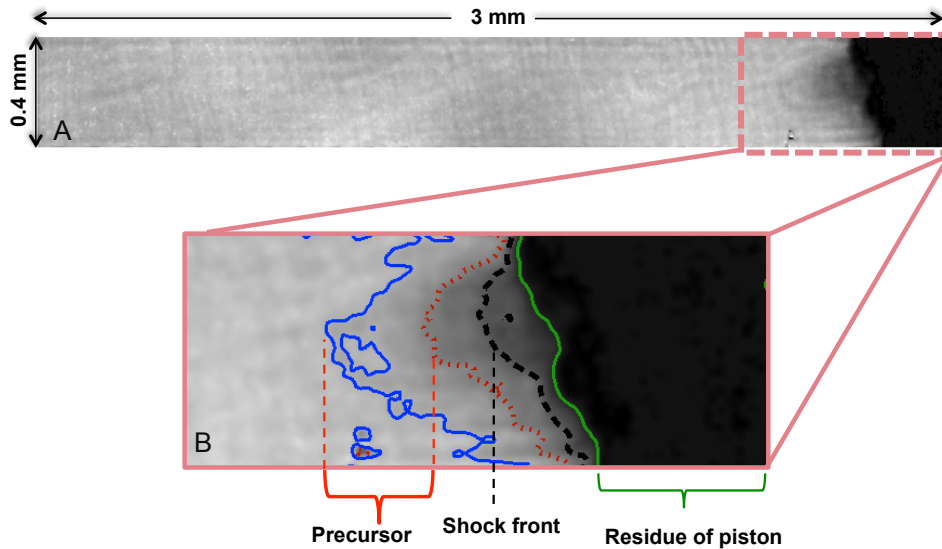


Fig. 2: A) Snapshot of the shock probed by the XRL laser at 21.2 nm. The imaging laser arrives 20 ns after the shock driving laser. The shock is moving from right to left. B) The enlarged radiograph through Si_3N_4 windows where different parts of shocks are identified.

In previous experiments (for instance (Bouquet et al. 2004; Stehlé et al. 2010)) visible interferometry demonstrated the presence of a radiative precursor with electron densities of $10^{18} - 10^{19} \text{ cm}^{-3}$. However, due to high electron density, the plasma in the shock front is opaque to visible light as well as the post shock is opaque to visible probing. At the probing wavelength of the XRL beam of 21.2 nm, the critical electron density of the plasma n_c ($2.5 \times 10^{24} \text{ cm}^{-3}$) is few hundreds times higher than the visible one, and thus, by using the XRL beam it is possible to probe these shock conditions. Another advantage of using the XRL beam is the instantaneous

imaging of the whole shock structure and the reduction of blurring effects due to refraction. However, residual blurring ($\sim 10 - 12 \mu\text{m}$) may still be present due to the plasma motion at a velocity of $50-60 \text{ km s}^{-1}$ during the short time ($\sim 0.2 \text{ ns}$) of the XRL beam.

Results from XRL probing the shock at 20 ns after its launching are reported in Fig. 2. The driving laser is coming from the right of the Fig. 2. The different parts of the shock are highlighted, with the help of color iso-contours, in Fig. 2B. The contours are normalized to maximum value of the signal after image processing. The darkest zone of the right side of the Fig. 2B corresponds to the residue of piston which is represented by green contour with normalized signal value of 0.2. The post shock and precursor regions are separated by black and blue color contour with normalized value of 0.4, and 0.8, respectively.

The shock front can be seen at a distance of about $400 \mu\text{m}$ from the right edge of the window. The edge of the Si_3N_4 window is located at a distance $\sim 0.55 \text{ mm}$ from the initial position of the piston. Thus, the shock front is located at a distance of $\sim 0.95 \text{ mm}$ from the initial position of the piston, which gives the mean shock velocity about $\sim 48 \text{ km s}^{-1}$. The thickness of the shock front at this time is about $10 - 20 \mu\text{m}$ which is comparable with the crossing time of the front in the field of view during XRL back-lighting.

3.2 Shock velocity from plasma self-emission

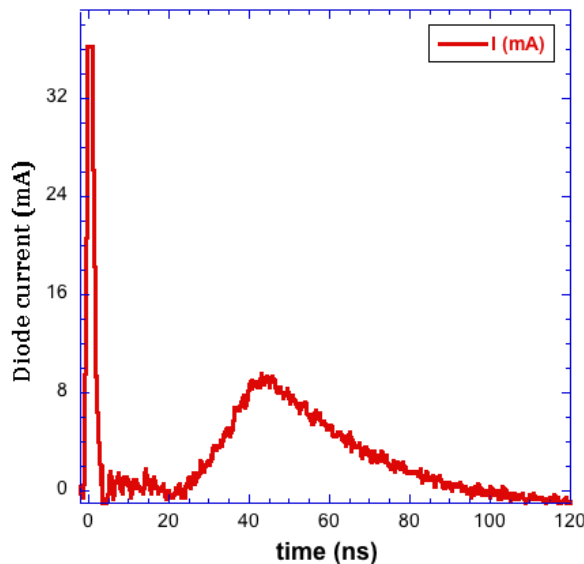


Fig. 3: XUV signal recorded by a diode placed side on which observes the plasma emission at a distance of $\sim 1.8 \text{ mm}$ from the initial position of the piston.

Results of the plasma self-emission in the XUV recorded with high-speed diodes are shown in Fig. 3. The results show a strong peak at $t = 0 \text{ ns}$, corresponding to the stray light emitted during the interaction of the AUX laser beam with the piston. Thus, this time can be chosen as zero, corresponding to the laser arrival on the target. The signal rises again sharply after $\sim 25 \text{ ns}$ and starts peak at 40 ns and then decreases slowly. This is consistent with the dynamics of shock front and post shock in the field of view of the diode. Thus the mean shock velocity at this position can be deduced from peak timing to $\sim 45 \text{ km s}^{-1}$, which is comparable with the measurement from XUV imaging at earlier time with the XRL beam.

4 Conclusions

We presented the results of a new experimental study of laser-generated radiative shocks focusing on two diagnostics: XUV instantaneous imaging at 21.2 nm and time and space resolved plasma self-emission using fast diodes. The results obtained from both diagnostics are consistent with each other indicating the shock velocity about 45 km s^{-1} which means upstream Mach number of about 250 (for the initial gas conditions at room temperature)(Drake 2006). The experiments show that the XRL probing is a promising tool to probe shock waves in general. The improvement in the quality of the imaging setup compared to the previous experiment (Stehlé et al. 2012b) enhanced the quality of image and allows to identify shock front without any ambiguity. A more detailed description of the shock parameters will be a subject of future experiments and publications.

The project has been funded by Observatoire de Paris, PNPS, UPMC, ANR-08-BLAN-0263-07 and LASERLAB access program. The authors acknowledge the contribution of the PALS technical staff, the target fabrication group of Observatoire de Paris, V. Petitbon (IPN) for the polystyrene manufacturing, F. Delmotte and E. Meltchakov for the XUV mirror fabrication. J. Prokúpek and M. Krůs acknowledge ELI: Extreme Light Infrastructure - project no. CZ.1.05/1.1.00/02.0061 and OPVK - project no. CZ.1.07/2.3.00/30.0057.

References

- Argiroffi, C., Maggio, A., & Peres, G. 2007, arXiv preprint astro-ph/0701765
- Bouquet, S., Stehlé, C., Koenig, M., et al. 2004, *Physical review letters*, 92, 225001
- Bouvier, J., Alencar, S. H. P., Boutelier, T., et al. 2007, *A&A*, 463, 1017
- Chaulagain, U., Stehlé, C., de Sá, L., et al. 2012, in *SF2A-2012: Proceedings of the Annual meeting of the French Society of Astronomy and Astrophysics*, Vol. 1, 305–307
- Commerçon, B., Audit, E., Chabrier, G., & Chièze, J.-P. 2011, *Astronomy & Astrophysics*, 530
- Doss, F., Robey, H., Drake, R., & Kuranz, C. 2009, *Physics of Plasmas*, 16, 112705
- Drake, R. P. 2006, *High-energy-density physics: fundamentals, inertial fusion, and experimental astrophysics* (Springer), pg.113
- González, M., Audit, E., & Stehlé, C. 2009, arXiv preprint arXiv:0902.1645
- Henke, B., Gullikson, E., & Davis, J. 1993, *Atomic Data and Nuclear Data Tables*, 54, 181
- Jungwirth, K., Cejnarova, A., Juha, L., et al. 2001, *Physics of Plasmas*, 8, 2495
- Reighard, A., Drake, R., Dammberg, K., et al. 2006, *Physics of Plasmas*, 13, 082901
- Rus, B., Mocek, T., Präg, A., et al. 2002, in *AIP Conference Proceedings*, Vol. 641, 182
- Stehlé, C., Champion, N., Delattre, P., et al. 2012a, *EAS Publications Series*, 58, 155
- Stehlé, C., González, M., Kozlova, M., et al. 2010, *Laser and particle beams*, 28, 253
- Stehlé, C., Kozlová, M., Larour, J., et al. 2012b, *Optics Communications*, 285, 64
- Stehlé, C., Lefevre, R., Chaulagain, U., et al. 2012c, in *ICXRL conf. Proc.*, Vol. 130
- Zeldovich, I. B. & Zel'dovich, Y. B. 2002, *Physics of shock waves and high-temperature hydrodynamic phenomena* (Courier Dover Publications)